Zeitschrift: Schweizerische mineralogische und petrographische Mitteilungen = Bulletin suisse de minéralogie et pétrographie

Band: 81 (2001)

Heft: 1

Artikel: Structural effects of OH => F subsituition in trioctahedral micas of the system : K2O-FeO-Fe2O3-Al2O3-SiO2-H2O-HF

Autor: Boukili, B. / Robert, J.-L. / Beny, J.-M.

DOI: https://doi.org/10.5169/seals-61680

SCHWEIZ. MINERAL. PETROGR. MITT. 81, 55–67, 2001

Structural effects of OH ⇒ F substitution in trioctahedral micas of the system: K_2O–FeO–Fe_2O_3–Al_2O_3–SiO_2–H_2O–HF

by *B. Boukili*[1], *J.-L. Robert*[2], *J.-M. Beny*[2] and *F. Holtz*[3]

Abstract

The OH ⇒ F substitution in trioctahedral ferrous micas has been investigated at 720 °C, 1 kbar P_{H_2O}, under fO_2 conditions set by the MW (Fe_2O_3–$Fe_{1-x}O$) buffer. The starting compositions belong to the annite-siderophyllite join: $K(Fe_{3-x}Al_x)(Si_{3-x}Al_{1+x})O_{10}(OH)_2$ with x = 0 (annite), 0.5 (Fe-eastonite), and 0.75 (Es). In F-bearing system, the compositions investigated belong to (OH,F)-annite, (OH,F)-Fe-eastonite and (OH,F)-Es joins. A single mica phase was observed for (OH,F)-annite in $0 \leq X_F \leq 0.5$ compositional range, and in $0 \leq X_F \leq 0.2$ range for (OH,F)-Fe-eastonite and (OH,F)-Es. Beyond these values, toward to F-rich compositions, topaz, quartz, magnetite and glass coexist with mica.

The correlation of the reticular distance d_{060} as a function of X_F shows that (OH,F)-annite and (OH,F)-Es behave differently as X_F increases. Mössbauer measurements along the annite and Es (OH,F) joins demonstrate that the Fe^{3+} content decreases from $X_{Fe^{3+}}$ (Fe^{3+}/Fe_{total}) = 9.1% for $X_{F\text{-}ann} = 0$ to 3.1% for $X_{F\text{-}ann} = 0.5$ and it increases slightly from $X_{Fe^{3+}} = 2.4\%$ at $X_{F\text{-}Es} = 0$ to 3% at $X_{F\text{-}Es} = 0.2$. FTIR spectroscopy in the far-infrared region (200–50 cm^{-1}) also shows an opposite trend wavenumber-shift between (OH,F)-annite and (OH,F)-Es with increasing X_F. In the single phase range, the band observed at 67 cm^{-1} in the (OH)-annite, corresponding to torsional vibration motion of the tetrahedral layer (mode III), shifts to higher wavenumbers with X_F. In contrast, this band (mode III) decreases from 91 cm^{-1} in the (OH)-Es end-member down to 88 cm^{-1} at $X_F = 0.2$. These shifts are related to changes in the K-site configuration, particularly to the variations of the tetrahedral rotation angle (α). The angle α increases from ≈ 2° for $X_{F\text{-}ann} = 0$ to 5.5° for $X_{F\text{-}ann} = 0.5$ and it decreases from 8.5° at $X_{F\text{-}Es} = 0$ to 5.3° at $X_{F\text{-}Es} = 0.2$.

The OH ⇒ F substitution induces local cationic changes and consequently a dimensional adaptation of sheets (limited in such micas to α = 5.5°), which in turn controls the fluorine solubility in these studied micas. The results also show that the Fe^{3+}/Fe_{total} ratio in F-bearing micas is not only controlled by fO_2 but also by structural constraints. The fluorine content of natural biotites has to be taken into account to estimate oxygen fugacities prevailing in the rocks.

Keywords: fluorine, trioctahedral ferrous micas, tetrahedral rotation (α), Mössbauer, FIR.

Introduction

Fluorine is a common constituent of biotite. It is well known that fluorine enhances the thermal stability of micas (MUNOZ, 1984). Knowledge of partition coefficients of fluorine between biotite and coexisting hydroxyl-bearing minerals or fluids is of importance in the earth sciences because it allows us to estimate the compositions of the fluid in terms of the fugacity ratio fH_2O/fHF and/or temperature (MUNOZ, 1969; MUNOZ and LUDINGTON, 1974). Fluorine is frequently involved in mineralization processes (e.g., Cu, Zn, Mo, Sn, Pb; TISCHENDORF, 1973; ZAW and CLARK, 1978; PARRY et al., 1978; GUNOW and MUNOZ, 1980; IMEOKPARIA, 1981) and modifies the physical and chemical properties of silicate melts (e.g., MANNING, 1981; DINGWELL et al., 1985). Thus, it is of particular interest to understand the OH ⇒ F substitution mechanism in biotite, which controls in turn the fluorine content in this mineral.

In view of the chemical complexity resulting from both cationic and anionic substitutions, numerous experimental studies have been performed on biotite coexisting with (OH,F)-fluids: stability and phase relations (MUNOZ and LUD-

[1] Faculté des sciences de Rabat-Agdal, Département des sciences de la Terre, UFR geoappl, BP 1014, Rabat, Maroc. <boukili@fsr.ac.ma>
[2] CNRS-CRSCM, Orléans, 45071-cedex 02, France.
[3] Universität Hannover, Institut für Mineralogie, Welfengarten 1, D-30167 Hannover, Deutschland.

INGTON, 1969, 1974; MUNOZ, 1984), synthesis and characterization of (OH,F)-bearing biotites by vibrational spectroscopy (LEVILLAIN, 1982; DYAR and BURNS, 1986; ROBERT et al., 1993), by NMR (SANZ and STONE, 1979, 1983), and by EXAFS (MANCEAU et al., 1990), and finally crystal-chemical approaches for modelling the OH ⇒ F substitution in biotite (MASON, 1992; ROBERT et al., 1993). The most important conclusions from these studies are that the OH ⇒ F substitution is mainly governed by (1) the activity of hydrofluoric acid (fHF) in the fluid in equilibrium with biotite, (2) temperature, (3) composition, in particular X_{Fe}, (4) the entropy of the OH ⇔ F exchange reaction between biotite and hydrothermal fluid, and (5) crystal-chemical constraints.

The present study contributes to the understanding of crystal-chemical constraints that are shown to play an important role for the incorporation of fluorine in biotite. The investigated micas are synthetic and belong to the annite-siderophyllite join. The analytical techniques used in this study are Mössbauer and far-infrared spectroscopy. Mössbauer spectroscopy is used to understand the role of the Fe^{3+} content and its distribution between octahedral and tetrahedral sheets, whereas far-infrared spectroscopy allows to track the evolution of interlayer geometry, which is related to the size differences between adjacent layers.

Experimental Methods

Starting materials were gels prepared according to the method of HAMILTON and HENDERSON (1968). Potassium was introduced as dried K_2CO_3 transformed to nitrate by nitric acid attack, silicon as tetraethyl orthosilicate (TEOS), aluminium and one part of iron (50%) as nitrate. Finally, fluorides (KF, AlF_3 or FeF_2 and metallic iron (Fe^o) were mechanically added to the gels to obtain the appropriate bulk compositions. The compositions of the trioctahedral F-free micas studied are expressed by:

$$K(Fe_{3-x}Al_x)(Si_{3-x}Al_{1+x})O_{10}(OH)_2$$

where x corresponds to the rate of the Tschermak-type substitution. The OH ⇒ F substitution has been studied along three (OH,F)-joins:

(OH,F)-annite:

$KFe_3(Si_3Al)O_{10}(OH,F)_2$; [x = 0]

(OH,F)-Fe-eastonite:

$K(Fe_{2.5}Al_{0.5})(Si_{2.5}Al_{1.5})O_{10}(OH,F)_2$; [x = 0.5]

(OH,F)-Es:

$K(Fe_{2.25}Al_{0.75})(Si_{2.25}Al_{1.75})O_{10}(OH,F)_2$; [x = 0.75]

The last join corresponds to a composition intermediate between Fe-eastonite (X = 0.5) and siderophyllite (X = 1).

Synthesis were done in Tuttle-type externally heated pressure vessels working vertically, with water as the pressure medium. Temperature was measured using Ni-NiCr thermocouples calibrated against the melting points of NaCl and $ZnCl_2$. Temperature uncertainty is less than ±5 °C. Pressures were measured with a Bourdon gauge, with an uncertainty of less than ±50 bars. All experiments were performed at 720 °C, 1 kbar P_{H_2O}, with a duration of 7 days. Oxygen fugacity was controlled by the double capsule method of EUGSTER (1957), using the magnetite-wüstite (MW) assemblage as a solid buffer introduced with water in the external Au-capsule. In the inner capsule ($Ag_{70}Pd_{30}$), the gels were introduced with 15 wt% distilled water added. The duration was not varied. However, synthesis experiments on other types of micas (Mg and Li-bearing micas) have shown that this duration is long enough to obtain equilibrium assemblages (e.g., ROBERT et al., 1989; 1993). Cooling was performed by removing the vessel from the furnace and a temperature of less than 100 °C was reached after less than 1 hour.

The run products were examined with a petrographic microscope and by scanning electron microscopy (SEM). X-ray diffraction was used to confirm the single phase character and to characterize the mica. Diffraction patterns were obtained between $5° \leq 2\theta \leq 65°$, the radiation used was Co-Kα (λ = 1.7902 Å). The interplanar distances d_{001} (= c sin β) and d_{060} (= b/6) were systematically measured using Si as an internal standard.

Infrared spectra were recorded on a Bruker IFS 113 spectrometer. Samples were prepared as pellets of 100 mg, composed of 30 wt% of the run product and 70 wt% polyethylene .

Mössbauer spectroscopy was performed using a constant acceleration spectrometer with a multichannel analyser (512 channels) in conjunction with an electromechanical drive system with a triangular velocity shape. All spectra were recorded at room temperature with a ^{57}Co in Rh source of 25 mCi nominal activity. The samples were mixed with senegal gum. Saturation effects were minimized by using samples containing 5 mg natural Fe/cm^2. The number of counts per channel was in the range $5 \cdot 10^6$ to $8 \cdot 10^6$. The results were calibrated against α-Fe foil. The spectra were fitted to the sum of lines of Lorentzian shape using the least-square fitting program (MOSS) of BONNIN and DESBARESS (1988, ESPCI-Paris). During the fitting process the linewidth of different ferrous doublets was kept equal but allowed to vary, the same procedure has been used for Fe^{3+}. The

octahedral sheet of ferrous biotite has two types of site, M1 and M2, adjacent to four oxygens and two (OH,F) groups. Trans-sites (M1) and cis-sites (M2) are distinguished with respect to the OH or F position. M1 and M2 sites can have different environments because of cationic substitutions. The hydroxyl group can also be substituted by fluorine or can be lost during oxidation (deprotonation or dehydrogenation process).

In the previous works, Mössbauer spectra of biotite were usually fitted with two ferrous doublets. During the fitting process, equally linewidth constraints for different doublets were a current procedure and the assignment of Fe^{2+} quadrupole doublets was done essentially on the basis of the relative areas of M1:M2 sites. In the case of annite (synthetic or natural samples) M1:M2 multiplicity ratios must be equal to 1:2 to be consistent with the structural data of HAZEN and BURNHAM (1973) which were obtained from a crystal with nearly annite end-member composition. However, this method of determination of site populations is questionable (SANZ, 1976; DYAR, 1987; RANCOURT, 1994). As shown by near infrared spectroscopy (BOUKILI et al., 1993; BOUKILI, 1995), synthetic annite is a solid solution with at least five end-members (annite, oxyannite, ferriannite, ferri-muscovite and ferri-siderophyllite). These chemical variations around Fe^{2+} may lead to a distribution of quadrupole splitting values, so the relative areas of M1:M2 sites may not be consistent with the the structural refinements of HAZEN and BURNHAM (1973). Therefore, it is impossible to determine the distribution of Fe^{2+} on M1:M2 sites from quadrupole splitting. Consequently, the problem of the assignment of the ferrous doublets will not be discussed in the present work. Only the Fe^{3+} content and its distribution between octahedral and tetrahedral sheets has been investigated, in order to determine whether or not the variations of d_{060} as a function of X_F are related to a variation of the Fe^{3+} content and/or distribution along the (OH,F)-annite and (OH,F)-Es joins.

Experimental products

The experimental products were composed of mica only (plus a fluid phase) or of mica and additionnal phases such as quartz, topaz, magnetite, glass. The presence of such minerals in addition to mica does not mean that the assemblages is metastable and does not result from kinetic problems. WEIDNER and MARTIN (1987) have shown that F-rich mica can coexist with melt, quartz and topaz at temperatures as low as 650 °C at 1 kbar. The cooling rate was also fast enough to allow to quench F-bearing melts as a glass in charges with high F-contents (no formation of quench-crystals). Thus, because the diffusivity of fluorine is at least as fast in melts than in micas, a reequilibration of the minerals (in particular F-content of micas) during cooling can also be excluded.

On the other hand several attempts were made to analyze the synthetic micas by electron microprobe, but they failed owing to the small grain size. However, in order to check the nominal values of X_F, wet chemical analyses have been done on 30 to 40 mg of the run products obtained along the (OH,F)-annite join. Only small deviations were observed from the nominal values of X_F (Tab. 1). In the present work, the (OH,F)-micas studied will be labeled on the basis of the bulk atomic fluorine fraction (X_F = F/OH+F) of the starting gels. It is emphasized that this value of X_F does not necessarily correspond to that of the synthesized micas (especially in run products composed of several phases which can also incorporate fluorine).

(OH,F)-ANNITE

A single mica phase was observed in the range $0 \leq X_F \leq 0.5$. The annite-(OH) end-member was found to have small amounts of the phases sanidine and magnetite (less than 1%). For $X_F \geq 0.6$, the mica coexists with topaz, quartz and a low refractive-index phase that is probably glass (Tab. 2). For the theoretical F-annite end-member ($X_F = 1$), the run product was a mixture of mica,

Tab. 1 Comparison of nominal and analysed fluorine content of the run products along the (OH,F)-annite join. Note: The analyses could not be duplicated because of the small amounts of available experimental products. The value marked by (*) is representative of error since (OH)-annite is F-free. Note that the F content for the F-free composition is not nil and that all values are slightly higher than the nominal wt% F. Thus, either the analytical technique was not perfectly calibrated or all the starting gels were not absolutely F-free (the first explanation is the most probable).

$KFe_3(Si_3Al)O_{10}(OH)_2$	X_F	wt% F nominal	wt% F wet chemistry
$(OH)_2$-annite	0	0.00	0.28*
$(OH_{1.6}F_{0.4})$-annite	0.2	1.47	1.88
$(OH_{1.2}F_{0.8})$-annite	0.4	2.90	2.93
(OH_1F_1)-annite	0.5	3.61	3.80
$(OH_{0.8}F_{1.2})$-annite	0.6	4.31	4.56
$(OH_{0.4}F_{1.6})$-annite	0.8	5.68	5.93
$(F)_2$-annite	1.0	7.02	7.12

topaz, glass and trace amounts of magnetite. Along the (OH,F)-annite join, crystal sizes of mica are less than 2 μm. The micas have a more and more pronounced clear green color as X_F increases (may be related to the variation of Fe^{3+}). Interplanar distances d_{001} and d_{060}, measured from X-ray diffraction patterns, decrease as the amount of fluorine in the system increases (Fig. 1). The apparent break in slope at $X_F = 0.5$–0.6 indicates the upper solubility limit of fluorine in annite and is related to the appearance of additionnal phases other than mica.

(OH,F)-FE-EASTONITE

On this join, a single mica phase was obtained for $0 \leq X_F \leq 0.2$, with a typical grain size of 1 to 2 μm. The color changes from grey for the (OH)-Fe-eastonite end-member to green-grey with increasing X_F. At $X_F > 0.2$, the quenched assemblage consists of mica, topaz, glass and quartz in very small amounts (Tab. 2). Quartz occurs in very small amounts. As previously observed on the (OH,F)-annite join, the reticular distances d_{001} decreases gradually as X_F increases (Fig. 1). This decrease is observed in the single phase range as well as for micas belonging to a polyphase assemblage. This suggests that the cationic composition of the mica changes along the join, especially in the multiphase assemblage. In contrast to the (OH,F)-annite join, d_{060} values vary only slightly for $0 \leq X_F \leq 0.2$, but increase for fluorine-rich bulk compositions.

(OH,F)-ES

(OH)-Es is the most aluminous mica that could be obtained along the annite-siderophyllite join, in agreement with the results of RUTHERFORD (1973). Fluorine solubility along the (OH,F)-Es join is restricted to $X_F = 0.2$. For more fluorine-rich compositions, mica occurs with topaz, glass and an unidentified phase that was determined to be an aluminum silicate by qualitative analysis (EDS, Tab. 2). As previously observed for annite and Fe-eastonite, the d_{001} distance decreases gradually as the fluorine content increases. By contrast, d_{060} increases with X_F from 0 to 0.2. A break is observed between $X_F = 0.2$. and 0.4 (Fig. 1). This behaviour, different from that observed for

Tab. 2 Compositions investigated and run products obtained at 720 °C, MW buffer and 1 kbar. Interplanar distances are measured at ±0.0004 Å. (α_1) tetragonal rotation angles are calculated from the relations of DONNAY et al. (1964), (α_2) from TATEYAMA et al. (1977). The lattice parameter b is calculated from ($b = 6 \times d_{060}$). The phases obtained are annite and aluminous biotite (Al-biotite), quartz (qtz), topaz (tpz), mica (mc), glass (gl) and non identified aluminous silicate crystalline phases (Si,Al). Parentheses: (...) indicate trace amounts.

Starting compositions	Phases obtained	d_{060}(Å)	d_{001}(Å)	b (Å)	α_1(°)	α_2(°)
(OH,F)-annite						
$KFe_3(Si_3Al)O_{10}(OH)_2$	annite	1.5568	10.1501	9.3408	–	2.19
$KFe_3(Si_3Al)O_{10}(OH_{1.6}F_{0.4})$	annite	1.5553	10.0920	9.3318	–	3.74
$KFe_3(Si_3Al)O_{10}(OH_{1.2}F_{0.8})$	annite	1.5539	10.0020	9.3234	1.466	4.90
$KFe_3(Si_3Al)O_{10}(OH_1F_1)$	annite	1.5522	9.9459	9.3132	3.05	–
$KFe_3(Si_3Al)O_{10}(OH_{0.8}F_{1.2})$	mc + (qtz)	1.5510	9.9807	9.3060	–	5.47
$KFe_3(Si_3Al)O_{10}(OH_{0.4}F_{1.6})$	mc+tpz+(qtz)+gl+(mt)	1.5528	9.9466	9.3168	2.60	7.32
$KFe_3(Si_3Al)O_{10}(F)_2$	mc+tpz+v+(mt)	1.5525	9.9479	9.3150	2.84	5.83
(OH,F)-Fe-eastonite						
$K(Fe_{2.5}Al_{0.5})(Si_{2.5}Al_{1.5})O_{10}(OH)_2$	Al-biotite	1.5500	10.0896	9.3000	9.94	4.39
$K(Fe_{2.5}Al_{0.5})(Si_{2.5}Al_{1.5})O_{10}(OH_{1.6}F_{0.4})$	Al-biotite	1.5502	9.9987	9.3012	9.90	5.31
$K(Fe_{2.5}Al_{0.5})(Si_{2.5}Al_{1.5})O_{10}(OH_{1.2}F_{0.8})$	mc+(qtz)	1.5526	9.9707	9.3156	9.38	4.78
$K(Fe_{2.5}Al_{0.5})(Si_{2.5}Al_{1.5})O_{10}(OH_{0.8}F_{1.2})$	mc+gl	1.5517	10.0037	9.3102	9.58	5.46
$K(Fe_{2.5}Al_{0.5})(Si_{2.5}Al_{1.5})O_{10}(OH_{0.4}F_{1.6})$	mc+tpz+gl	1.5549	9.9531	9.3294	8.85	4.71
$K(Fe_{2.5}Al_{0.5})(Si_{2.5}Al_{1.5})O_{10}(F)_2$	mc+tpz+gl	1.5552	9.9441	9.3312	8.87	5.28
(OH,F)-Es						
$K(Fe_{2.25}Al_{0.7})(Si_{2.25}Al_{1.75})O_{10}(OH)_2$	Al-biotite	1.5458	10.0594	9.2748	12.48	8.48
$K(Fe_{2.25}Al_{0.75})(Si_{2.25}Al_{1.75})O_{10}(OH_{1.6}F_{0.4})$	Al-biotite	1.5486	10.0017	9.2916	12.01	5.25
$K(Fe_{2.25}Al_{0.75})(Si_{2.25}Al_{1.75})O_{10}(OH_{1.2}F_{0.8})$	mc+gl	1.5476	10.0234	9.2856	12.18	7.13
$K(Fe_{2.25}Al_{0.75})(Si_{2.25}Al_{1.75})O_{10}(OH_{0.8}F_{1.2})$	mc+tpz+gl	1.5569	9.9766	9.3414	10.47	4.51
$K(Fe_{2.25}Al_{0.75})(Si_{2.25}Al_{1.75})O_{10}(OH_{0.4}F_{1.6})$	mc+gl+tpz+(AlSi?)	1.5545	9.9233	9.327	10.93	5.00
$K(Fe_{2.25}Al_{0.75})(Si_{2.25}Al_{1.75})O_{10}(F)_2$	mc+gl+tpz+(AlSi?)	1.5534	9.9508	9.3204	11.14	5.92

(OH,F)-annite, is particularly important and will be discussed below.

These results show that the solubility of fluorine is low in all investigated micas. In annite, fluorine solubility is attained at $X_{ann\text{-}F} = 0.5$, and it is more restricted for aluminous compositions at $X_{Al\text{-}bio\text{-}F} = 0.2$. In the case of annite, these results are in agreement with those obtained by MUNOZ and LUDINGTON (1974) at nearly similar experimental conditions. However, for more aluminous compositions our findings differ from those of MUNOZ and LUDINGTON (1974) who suggested that octahedral aluminum does not influence the OH ⇒ F substitution in ferrous biotite. In fact, there is an inverse correlation between octahedral aluminum and fluorine content in the micas that may be due to the Al-F avoidance rule. Aluminum should be less likely than Fe to seek F bonds over OH bonds (RAMBERG, 1952).

The most important feature observed by XRD is the inverse behaviour of d_{060} as a function of X_F, for micas along the (OH,F)-annite and the (OH,F)-Es joins (Fig. 1). Micas of the (OH,F)-Fe-eastonite join exhibit an intermediate behaviour. It is known that the cell parameter b ($= 6 \times d_{060}$) is related to both the T–O distance (d_t) in the tetrahedron, and the ditrigonal rotation angle α of tetrahedra, by the relation $b = 4\, d_t \sqrt{2} \cos \alpha$, which is valid for 1M trioctahedral micas (DONNAY et al., 1964). Therefore, the variations of b can be related either to variations of d_t, to variations of α, or both. The observed variations of b can therefore be related to changes in cationic composition or distribution between layers (e.g., Fe^{3+}) and/or to dimensional rearrangements induced by the OH ⇒ F substitution itself.

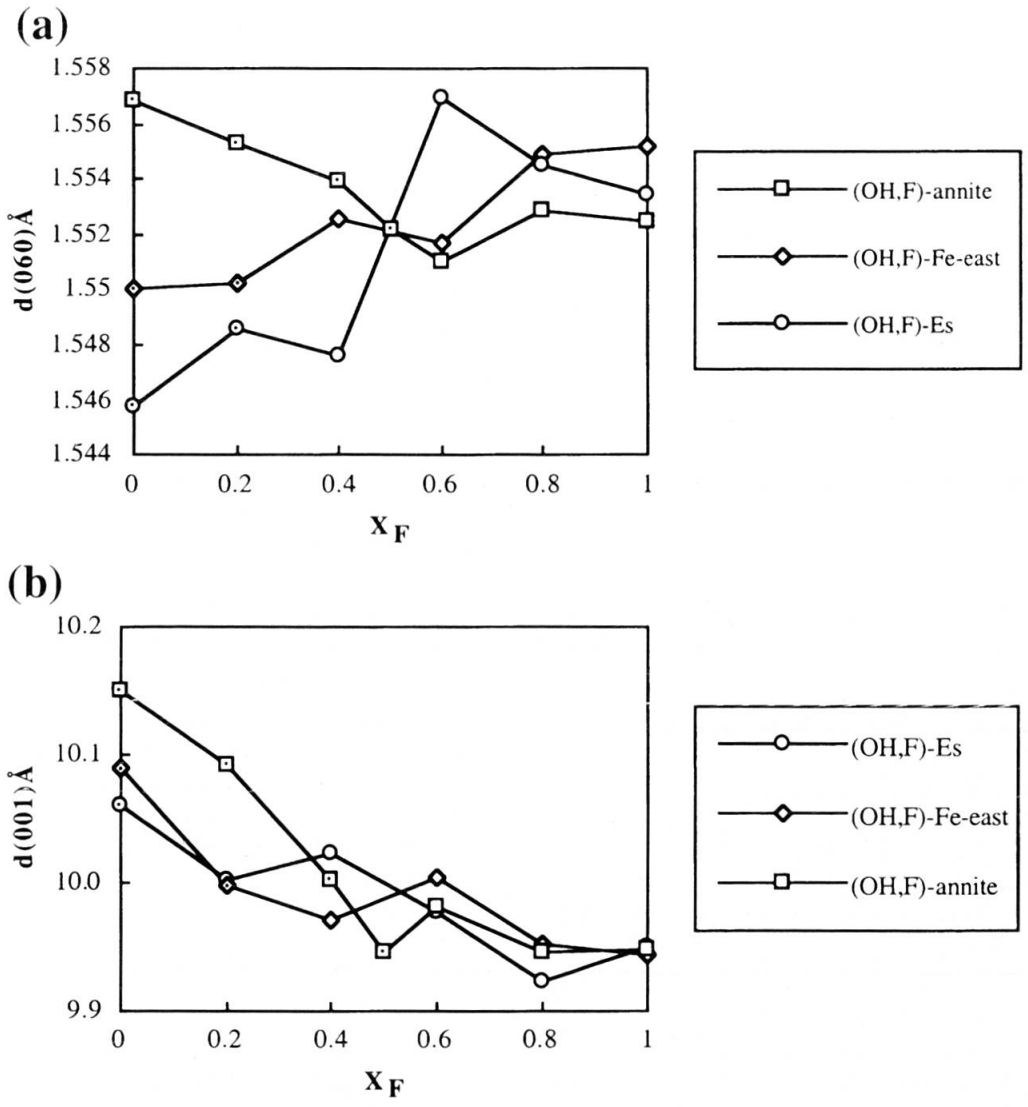

Fig. 1 Variations of measured interplanar distances d_{060} and d_{001} (in Å) ± 0.0004 versus nominal fluorine content (X_F) of the studied micas. Dotted symbols denote samples composed of mica only.

Tab. 3 Mössbauer parameters of (OH,F)-annite and (OH,F)-Es synthesized at 720 °C, MW buffer and 1 kbar. QS = Quadrupole splitting, δ = isomer shift and FWHM = full width at half maximum. QS, δ and FWHM are given in mm/s (±0.02 mm/s). $^{[a,b,c,d]}Fe^{2+}$ refers to the four octahedral ferrous environments observed. χ^2 is the statistical parameter commonly used to evaluate Mössbauer fits. (*) denotes samples composed of mica only.

	$^{[6]}Fe^{2+}$			$^{[6]}Fe^{3+}$			$^{[4]}Fe^{3+}$			χ^2
	δ	Q.S	FWHM	δ	Q.S	L_{mh}	δ	Q.S	L_{mh}	
(OH_2)-annite*	[a]- 1.12 [b]- 1.13 [c]- 1.11	2.44 2.25 2.63	0.30 0.33 0.26	0.43	0.88	0.43	0.20	0.49	0.30	1.09
$(OH_{1.6}F_{0.4})$-annite*	[a] 1.122 [b] 1.124 [c] 1.12	2.30 1.86 2.62	0.28 0.40 0.26	0.28	0.50	0.46	0.21	0.35	0.30	1.18
$(OH_{1.4}F_{0.6})$-annite*	[a]- 1.16 [b]- 1.14 [c]- 1.118 [d]- 1.117	2.22 1.91 2.51 1.45	0.30 0.35 0.29 0.35	0.34	0.58	0.32	0.23	0.45	0.32	0.98
(OH_1F_1)-annite*	[a]-1.14 [b]-1.14 [c]-1.11 [d]-1.16	2.18 1.84 2.43 1.36	0.29 0.32 0.28 0.32	0.36	0.45	0.32	–	–	–	0.96
$(OH_{0.4}F_{1.6})$-annite	[a]-1.14 [b]-1.16 [c]-1.15 [d]-1.19	2.12 1.72 2.40 1.33	0.28 0.42 0.27 0.32	0.25	0.84	0.4	0.20	0.35	0.32	1.67
(OH_2)-Es*	[a]-1.12 [b]-1.10 [c]-1.12	2.45 1.94 2.64	0.27 0.50 0.26	0.54	0.54	0.40	–	–	–	1.02
$(OH_{1.6}F_{0.4})$-Es*	[a]-1.15 [b]-1.13 [c]-1.12	2.25 1.82 2.57	0.28 0.44 0.27	0.37	0.45	0.32	–	–	–	1.09
$(OH_{1.4}F_{0.6})$-Es	[a]-1.14 [b]-1.10 [c]-1.12 [d]-1.06	2.24 1.86 2.56 1.40	0.28 0.29 0.28 0.29	0.35	0.34	0.32	–	–	–	1.27

Mössbauer spectroscopy data

(OH,F)-ANNITE

The effect of OH ⇒ F substitution on the Mössbauer spectra of annite is significantly different from all the other possible ionic substitutions in annite (Al^{3+} seems to produce the same effect). The fit results obtained without constraints on the FWHM (full width at half-maximum) are given in table 3. The spectra could not be fitted with two ferrous doublets. For $X_F \leq 0.2$, the spectra were fitted with three ferrous doublets, yielding Mössbauer parameters that are typical of octahedral Fe^{2+} (Tab. 3). For more F-rich mica, $0.2 < X_F \leq 0.5$, four ferrous components were required to fit correctly the experimental data. At $X_F = 0.8$ (this sample is not pure annite, see table 2), three ferrous doublets were required to fit the spectrum. Two ferric doublets were identified for $X_F = 0$. Mössbauer parameters (Tab. 3) are typical for octahedral Fe^{3+} (δ = 0.43 mm/s; Δ = 0.88 mm/s), and Fe^{3+} tetracoordinated (δ = 0.20 mm/s; Δ = 0.49 mm/s) as proposed by ANNERSTEN et al. (1971). For $X_F > 0$, the fits need only one ferric doublet corresponding to octahedral Fe^{3+}. The total Fe^{3+} content decreases with increasing X_F in the compositional range $0 \leq X_F \leq 0.5$ (Fig. 2, Tab. 4). Similar results have been obtained by RANCOURT et al. (1995). It is noteworthy that the effects induced by the OH ⇒ F substitution in annite (decrease of the total Fe^{3+} content, and disappearance of $^{[4]}Fe^{3+}$) are similar to those of the Al-Tschermak substitution, along the annite-siderophyllite join (BOUKILI et al., 1993).

ES-(OH,F)

The spectra of three samples with $0 \leq X_F \leq 0.4$ have been collected (Fig. 3). Only samples with X_F of 0 and 0.2 are pure micas. Three ferrous doublets were required to fit the Mössbauer spectrum of the OH-end-member, whereas for more F-rich

Tab. 4 Relative areas (± 1%) obtained from Mössbauer fitted spectra of (OH,F)-annite and (OH,F)-Es. (*) denotes samples composed of mica only.

	$^{[6]}Fe^{2+}$				$^{[6]}Fe^{3+}$	$^{[4]}Fe^{3+}$	Fe^{3+}_T
areas (%)	$^{[c]}Fe^{2+}$	$^{[d]}Fe^{2+}$	$^{[a]}Fe^{2+}$	$^{[b]}Fe^{2+}$			
$(OH)_2$-annite*	34.3	–	43.2	13.4	2.9	6.2	9.1
$(OH_{1.6}F_{0.4})$-annite*	33.5	–	36.0	25.00	1.8	3.4	5.3
$(OH_{1.2}F_{0.8})$-annite*	24.4	9.0	35.0	27.17	2.0	2.2	4.2
(OH_1F_1)-annite*	22.3	12.7	36.2	25.46	3.1	-	3.1
$(OH_{0.8}F_{1.2})$-annite	21.5	14.1	32.2	25.81	2.8	3.5	6.3
$(OH)_2$-Es*	40.9	–	37.9	18.62	2.4	–	2.4
$(OH_{1.6}F_{0.4})$-Es*	41.9	–	33.7	21.93	3.0	–	3.0
$(OH_{1.2}F_{0.8})$-Es	31.3	10.3	39.9	15.51	2.8	–	2.8

compositions (X_F = 0.2 and 0.4), the spectra were fitted with four ferrous components. One ferric doublet was observed and assigned to $^{[6]}Fe^{3+}$. At X_F = 0.2, the measured Fe^{3+} content is slightly higher than that of the (OH)-Es end-member (Fig. 2, Tab. 4). The Fe^{3+} content of (OH)-Es end-member is clearly lower than that of the (OH)-annite end-member, so Al^{3+} seems to play the same structural role as fluorine.

Considering the oxidation state of the micas studied, in the single phase domain, the trends of the d_{060} against X_F reflect the variation of the Fe^{3+} content of micas as already suggested in the pioneering works of WONES (1963 a, b). In the case of annite, the Fe^{3+} content decreases as X_F increases [for single-phase samples: decrease from 9.1 to 3.1% Fe^{3+} from annite-$(OH)_2$ to annite-(OH_1F_1)], whereas Es-(OH,F) shows a slightly opposite trend [for single-phase samples: increase from 2.4 to 3.0% Fe^{3+} from Es-$(OH)_2$ to Es-$(OH_{1.6}F_{0.4})$]. Usually, variations of the Fe^{3+} content are considered to be due to changes of the oxygen fugacity. In this study, the oxygen fugacity was kept constant using solid-state buffers, therefore the variation of Fe^{3+} content is difficult to explain.

– The possible effect of water activity on the Fe^{3+} content must be ruled out because all experiments were performed under water-saturated conditions.

– Another possibility is that the OH ⇒ F substitution reduces the number of hydroxyl groups that can be deprotoned at imposed fO_2. This may explain the decrease of the Fe^{3+} content along the (OH,F)-annite join as a function of X_F, but it cannot explain the opposite behaviour observed for (OH,F)-Es. Thus, this explanation alone cannot account for the behaviour of both (OH,F)-annite and (OH,F)-Es.

– An additional explanation is that the variations of Fe^{3+} contents of the micas are controlled by structural or geometrical constraints due to the incorporation of fluorine into the structure (in

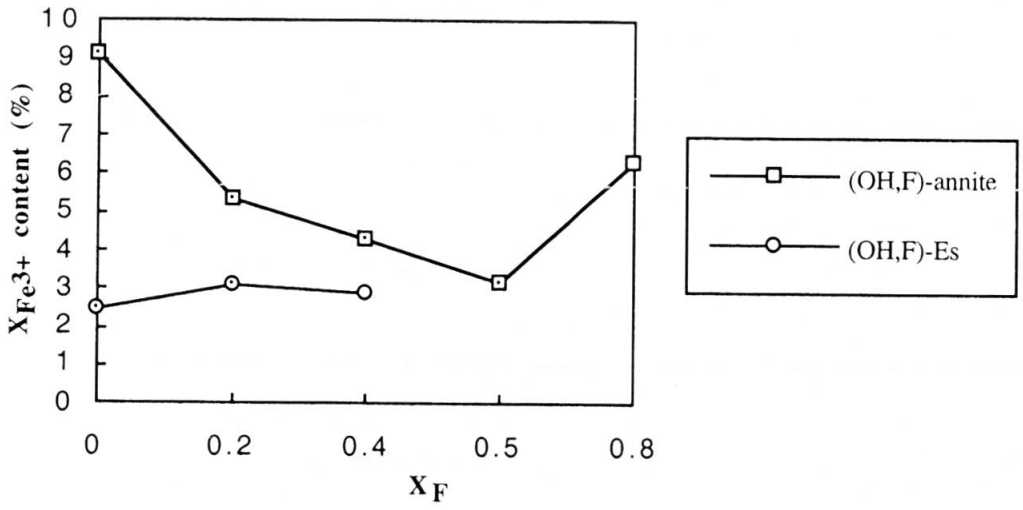

Fig. 2 Relationship between $X_{Fe^{3+}}$ (= Fe^{3+}/Fe_{total}) content (in %) obtained from Mössbauer measurements versus nominal X_F. Dotted symbols denote samples composed of mica only.

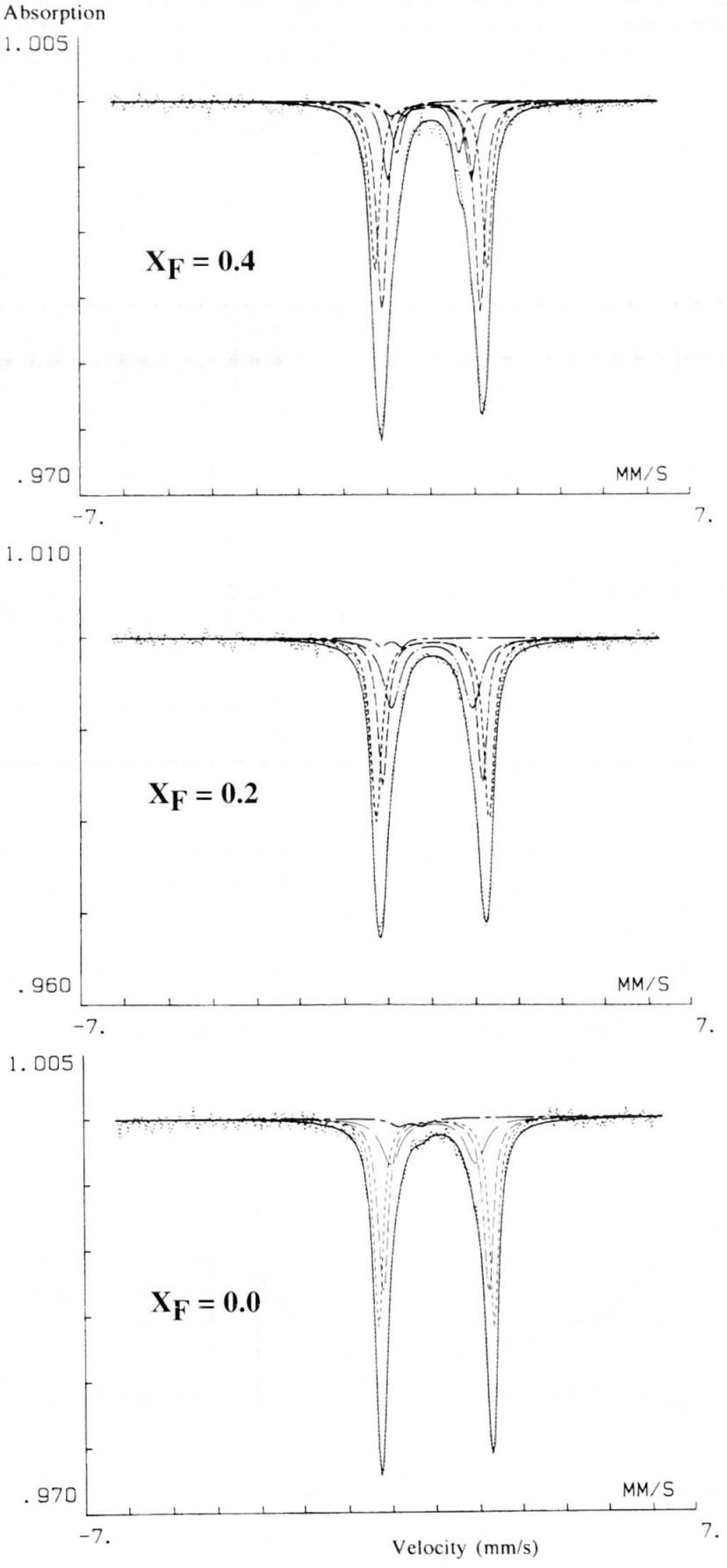

Fig. 3 Mössbauer spectra of (OH,F)-Es. Zero velocity is defined as the position of the centroid in iron metal.

agreement with results of previous studies; e.g., GOODMAN and WILSON, 1973; FERROW, 1987; EARLY et al., 1995). It is known that the mismatch between sheets in trioctahedral micas is strongly correlated to cation radii and to the lattice parameter *b*, and that there exists a geometrical limit for possible trioctahedral mica structures (HAZEN and WONES, 1972, 1978). The OH ⇒ F substitution gives rise, as with cationic exchanges, to size differences between tetrahedral and octahedral sheets. This phenomenon is illustrated by the variations of d_{060}, d_{001} as X_F increases. It is also known that the tetrahedral rotation (α) accommodates the misfit between octahedral and tetrahedral layers, α being nearly equal to 0° (1.5°) in the case of annite (HAZEN and BURNHAM, 1973) and always lower than 12° as found in natural biotite (GUIDOTTI et al., 1975). These values of tetrahedral rotation angles represent the geometrical limit of stable trioctahedral potassium micas. Far-infrared spectroscopic investigations of these micas should test this explanation since a relation between K-O_{inner} bond length (inner: refers to the oxygens that are close to the interlayer cation) and tetrahedral rotation angle α has already been established (TATEYAMA et al., 1977).

Far-infrared data in the range (200–50 cm^{-1})

The calculations made by ISHII et al. (1967) on the idealized structure of potassium micas allow assignments of the bands appearing in the range (200–50 cm^{-1}) to interlayer vibrations. Their results show that the bands observed at wavenumbers higher than 130 cm^{-1} are due to lattice vibrations, whereas at lower wavenumbers, three translational vibrations (mode I, II, IV; LAPERCHE, 1991) and one torsional mode of the tetrahedral layer (mode III) are expected. The latter mode (III) involves basal oxygen vibrations around the interlayer cation. ISHII et al. (1967, 1969) reported far-infrared absorption spectra of natural and synthetic micas and assigned the strong bands occurring in the 120–60 cm^{-1} region to K–O stretching vibrations. The same assignment was given by TATEYAMA et al. (1977) for bands in the range 108–71 cm^{-1} observed in potassium micas. In addition, FARMER (1974) analysed far-infrared spectra of phlogopite and muscovite and also assigned the bands at 144 cm^{-1} and 150 cm^{-1} to out-of-plane K-O vibrations. The assignments adopted in this study are based on the above cited studies and also on that of LAPERCHE (1991), who used dichroism absorption effects on oriented crystals and polarized IR radiation to ascertain the assignments.

(OH,F)-ANNITE

The infrared spectra for all synthesized samples (pure micas and micas in polyphased products, see table 2) are shown in figure 4a. The band at 67 cm^{-1} in the OH-annite end-member shifts to higher wavenumbers with increasing X_F up to $X_F = 0.6$. For compositions with higher fluorine contents, the wavenumbers vary weakly (Fig. 5). This is interpreted as the result of the restricted fluorine solubility in annite (although the nominal X_F of the charge increases, the F-content of the mica does not change any more for $X_F > 0.6$ because of the presence of additional F-bearing phases). This band is absent in the spectra of talc and pyrophyllite (ISHII, 1967), whereas it occurs at 90 cm^{-1} and 108 cm^{-1} in phlogopite and muscovite, respectively. LAPERCHE (1991) attributed this band to mode III.

At higher wavenumbers, at least two bands are distinguished in the range 130–120 cm^{-1} at $X_F = 0$. As the fluorine content increases, the variations in wavenumber are weak. The two bands can be more clearly distinguished at high X_F. LAPERCHE (1991) assigned these two bands to translational vibrations of potassium in the *(a,b)*-plane. Finally two additional low-intensity bands, at around 154 and 160 cm^{-1}, may be related to the lattice-layer vibrations.

(OH,F)-FE-EASTONITE AND (OH,F)-ES

The bands that occur at 67 cm^{-1} in (OH)-annite shift to 77 cm^{-1} in (OH)-Fe-eastonite and 91 cm^{-1} for (OH)-Es end-members (Fig. 4 b, c). The band at 77 cm^{-1} shifts to 84 cm^{-1} at $X_{F\text{-east}} = 0.2$ and its wavenumber remains constant above $X_F = 0.2$ (Fig. 5). For the more Al-rich composition (Es), the band at 91 cm^{-1} shifts to a lower wavenumber at 88 cm^{-1} with increasing X_F from 0 to 0.2 in the pure mica samples and varies between 82 and 88 cm^{-1} in polyphased assemblages, as fluorine increases. For samples composed of pure micas, the evolution of wavenumber with increasing X_F shows an opposite behaviour between (OH,F)-annite, (OH,F)-Fe-eastonite compared to (OH,F)-Es. In figure 5, the break observed for the Es curve in the range $X_F = 0.2$ to 0.4 corresponds to the upper solubility limit of fluorine.

At higher wavenumbers, the effect of fluorine on the bands at 135–120 cm^{-1} is not clear, owing to a poor spectral resolution. The band positioned at 120–135 cm^{-1} becomes slightly wider because of the splitting of bands (Mode I and II) as X_F increases.

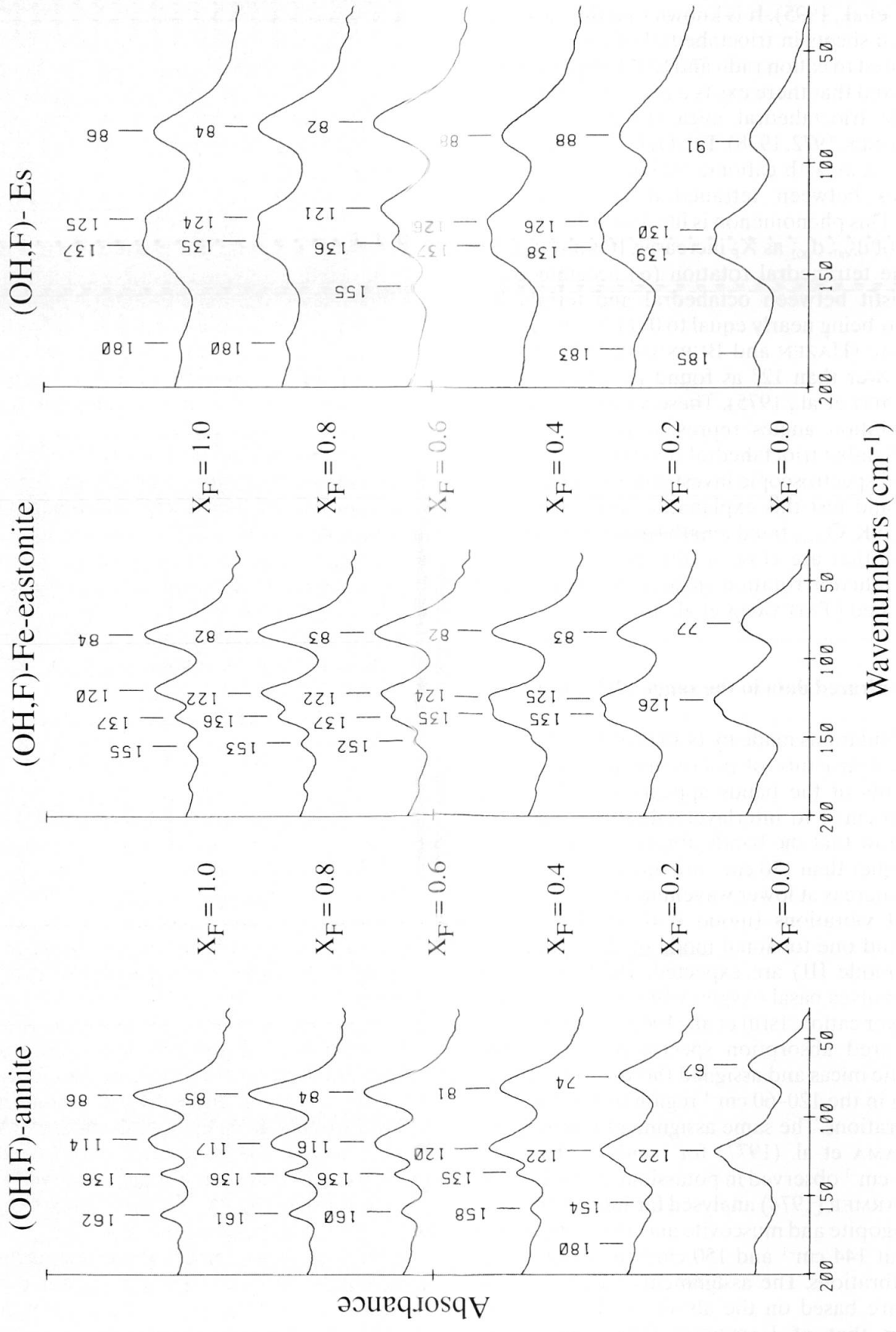

Fig. 4 Infrared absorption spectra of (a) (OH,F)-annite, (b) (OH,F)-Fe-eastonite, (c) (OH,F)-Es between 200 and 50 cm^{-1}.

Discussion

TATEYAMA et al. (1977) have established relations between the short K-O (inner) bond length (Å), the wavenumber of the torsional motion (cm^{-1}), the ditrigonal rotation angle α of tetrahedra (°), and the cell parameter *b* (Å):

(1) $d_{(K-O)short} = 3.676 - 0.0076 \times \nu_{K-O}$ (Å)

(2)

$$\alpha = \arctan\left(\sqrt{3} - \frac{6 \times \sqrt{d_{(K-O)}^2 - 0.25 \times [(d_{001} - 6.642)^2]}}{b}\right) \quad (°)$$

The use of these relationships with our (OH,F)-micas suggests that the K-O bond length shortens as X_F increases in annite and Fe-eastonite (see evolution in figure 6a for samples composed of micas only). (OH,F)-Es shows an opposite behaviour indicating that the short K-O bond length increases with X_F. Figure 6b shows the α values calculated from equation (2). In this figure, the contrasted behaviour of (OH,F)-annite and (OH,F)-Fe-eastonite on one hand, and of (OH,F)-Es on the other hand is also evident. The α angle increases from ≈ 2° for $X_F = 0$ to 5.5° for $X_F = 0.5$ in annite. In (OH,F)-Es, it decreases from 8.5° at $X_F = 0$ to 5.3° at $X_F = 0.2$.

The evolution of far-infrared K-O stretching wavenumbers (Mode III) in the (OH,F)-micas of this work is related to the variations of geometry of the interlayer site. The interlayer cavity is approximately hexagonal in the case of (OH,F)-annite owing to the weak dimensional misfit between the octahedral and tetrahedral sheets. As fluorine is incorporated into annite, the tetrahedral rotation angle increases. The OH ⇒ F substitution increases the dimensional misfit between the sheets. The hypothetical $Fe^{2+}O_4(OH)_2$ sheet may have a larger lateral extension than the octahedral $Fe^{2+}O_4(F)_2$ one as suggested by the evolution of lattice parameter *b* as a function of X_F (Tab. 2). The misfit of the tetrahedral sheet at $X_F = 0$ is alleviated by the incorporation of Fe^{3+} (RANCOURT et al., 1995).

When compared to (OH,F)-annite, (OH,F)-Es shows an opposite behaviour as the composition of mica increases in fluorine ($X_F = 0.2$). The ditrigonal potassium site is in a maximum state of distortion at (OH)-Es end-member composition (α = 8.5°). When fluorine enters the structure, the dimensional adjustments of the sheets operate by opening the interlayer cavity. The misfit between the octahedral and tetrahedral sheet is re-established by increasing the Fe^{3+} content at $X_{Es\text{-}F} = 0.2$. This dimensional adaptation is limited down to α = 5.35°, which is nearly the same value as obtained in $X_{ann\text{-}F} = 0.5$.

Conclusion

This study agrees with earlier works and shows that the fluorine contents and thereby the oxidation state of micas are controlled by structural factors. The Al-fluorine avoidance rule certainly has an important effect on the local distribution of iron in the octahedral sheets but does not play a determining role on the fluorine content of the micas. The fluorine solubility mainly depends on the ability of dimensional adaptation.

In petrological studies, biotite compositions are often projected onto the triangular diagram Fe^{2+}–Fe^{3+}–Mg of EUGSTER and WONES (1965) to estimate oxygen fugacities prevailing in the rocks. This study shows that crystal-chemical constraints also exert a major influence on Fe^{3+} contents. The use of this diagram for accurate oxygen fugacity determinations must be reconsidered for fluorine-bearing micas. For example, an increase of fluorine content from 0 to 1.5 wt% F (corresponding to an increase of X_F from 0 to 0.2) in annite

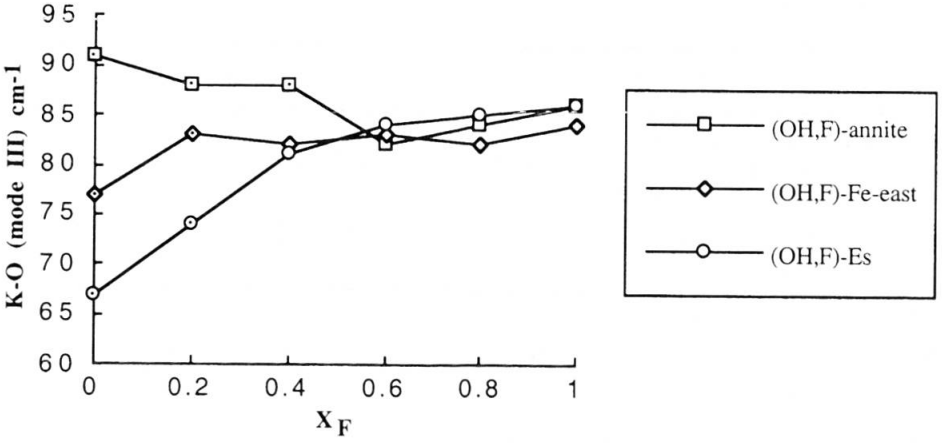

Fig. 5 Evolution of K-O stretching wavenumbers in cm^{-1} (mode III) of the micas of this work as a function of nominal X_F. Dotted symbols denote samples composed of mica only.

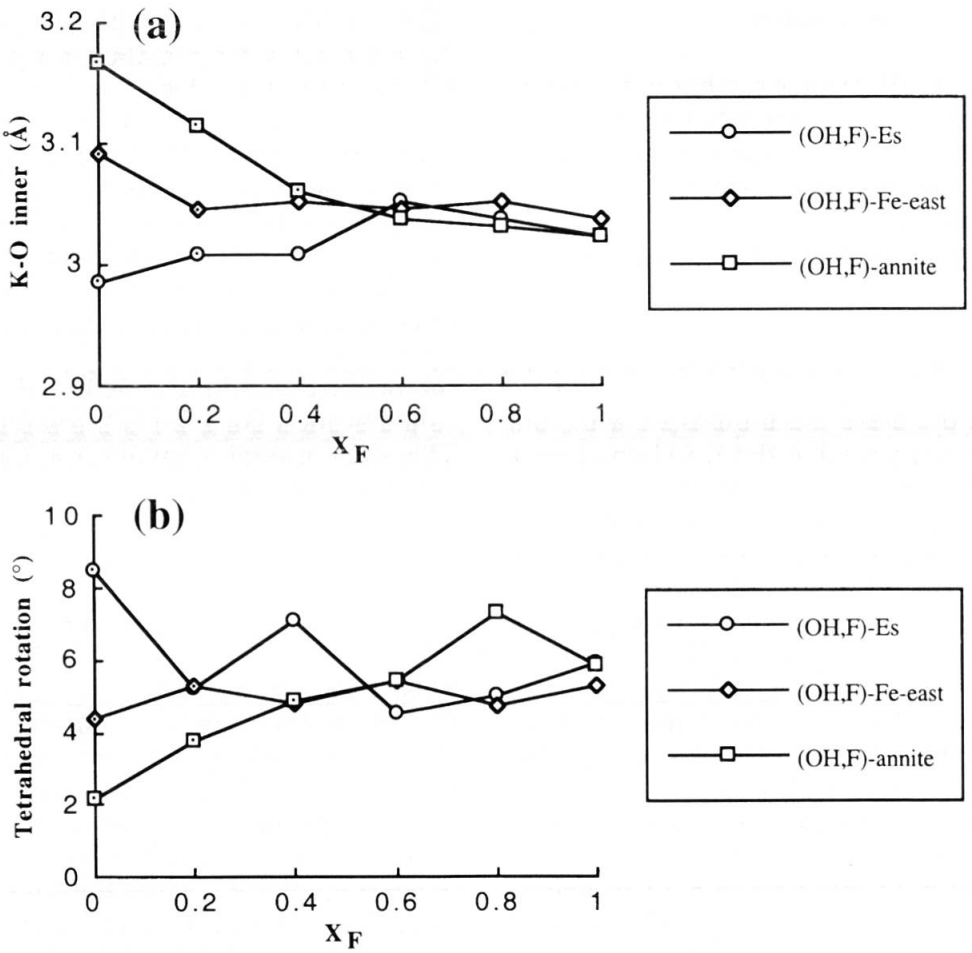

Fig. 6 (a) Variation of calculated K-O_{inner} distance versus nominal fluorine content of the micas studied. O_{inner}: inner oxygens, which are close to the interlayer cation (TATEYAMA et al., 1977). (b) Relationship between calculated tetrahedral rotation angles and X_F. Tetragonal rotation angles (α_2) are calculated from the relation proposed by TATEYAMA et al. (1977). Dotted symbols denote samples composed of mica only.

induces a decrease of the Fe^{3+} content of approximately 50% whereas it produces an increase of Fe^{3+} of 15% in an aluminous-annite (composition Es). The fluorine content has to be taken into account to estimate oxygen fugacities using triangular diagrams such that of EUGSTER and WONES (1965).

Acknowledgements

The authors thank Dr. V. Laperche (INRA-Versailles) for her assistance by collecting far-infrared spectra. Prof. D. Bonnin (Lab. de physique quantique, ESPCI-Paris) is gratefully acknowledged for his help and for providing the MOSS program. We are grateful to M.D. Dyar and R. Mason for careful reviews of this manuscript.

References

ANNERSTEN, H., DEVANARGANAN, S., HAGGSTROM, L. and WAPPLING, R. (1971): Mössbauer study of synthetic ferri-phlogopite $KMg_3Fe^{3+}Si_3O_{10}(OH)_2$. Phys. Stat. Solid., B48, K137–K138.

BOUKILI, B (1995): Cristallochimie des biotites ferro-alumineuses dans le système: Na_2O–K_2O–FeO–Fe_2O_3–Al_2O_3–SiO_2–H_2O–HF. Analyse par spectrométries vibrationnelles et Mössbauer. Thèse, Univ. Orléans, 320 pp.

BOUKILI, B., ROBERT, J.-L. and LAPERCHE, V. (1993): Solid solution range and crystal chemical characterization of trioctahedral micas in the system: K_2O–FeO–Fe_2O_3–Al_2O_3–SiO_2–H_2O–HF, at 600 °C, 1kbar. Terra Abstracts., 5, 485.

DONNAY, G., DONNAY, J.D.H. and TAKEDA, H. (1964): Trioctahedral one-layer Micas. II. Prediction of the structure from composition and cell dimensions. Acta Cryst., 17, 1341–1381.

DINGWELL, D.B, SCARFE, C.M. and CRONIN, D.J. (1985): The effect of fluorine on viscosities in the system Na_2O–Al_2O_3–SiO_2: Implications for phonolites, trachytes and rhyolites. Am. Mineral., 70, 80–87.

DYAR, M.D. and BURNS, R.G. (1986): Mössbauer spectral study of ferruginous one-layer trioctahedral micas. Am. Mineral., 71, 951–961.

DYAR, M.D. (1987): A review of Mössbauer data on trioctahedral micas: Evidence for tetrahedral Fe^{3+} and cation ordering. Am. Mineral., 72, 792–800.

EARLY III, D., DYAR, M.D., ILTON, E.S. and GRANTHEM, A.A. (1995): The influence of structural fluorine on biotite oxidation in copper-bearing aqueous solutions at low temperatures and pressures. Geochim. Cosmochim. Acta, 59, 2423–2433.

EUGSTER, H.P. (1957): Heterogeneous reactions involving oxidation and reduction at high pressures and temperatures. J. Chem. Phys., 26, 1760–1761.

FARMER, V.C. (1974): The layer silicates. In: FARMER, V.C. (ed.): The infrared spectra of minerals. Mineral. Soc. Great Britain, London, 331–363.

FERROW, E. (1987): Mössbauer and X-ray studies on the oxidation of annite and ferriannite. Phys. Chem. Mineral., 14, 270–275

GOODMAN, B.A. and WILSON, M.J. (1973): A study of the weathering of biotite using the Mössbauer effect. Mineral. Mag., 39, 448–454.

GUIDOTTI, C.V. (1984): Micas in metamorphic rocks. In: S.W. BAILEY (ed.): Reviews in Mineralogy, 13, Micas, 357–467.

GUIDOTTI, C.V., CHENEY, J.T. and CANTORE, P.D. (1975): Inter-relationship between Mg/Fe ratio and octahedral Al content in biotite. Am. Mineral., 60, 849–853.

GUNOW, A.J., LUDINGTON, S. and MUNOZ, J.L. (1980): Fluorine in micas from Henderson molybdenite deposit, Colorado. Econ. Geol., 75, 1127–1137.

HAMILTON, D.L. and HENDERSON, C.B.M. (1968): The preparation of silicate compositions by a gelling method. Mineral. Mag., 36, 632–838.

HAZEN, R.M. and BURNHAM, C.W. (1973): The crystal structure of one-layer phlogopite and annite. Am. Mineral., 58, 889–900.

HAZEN, R.M. and WONES, D.R. (1972): The effect of cations substitutions on the physical properties of trioctahedral micas. Am. Mineral., 57, 103–129.

HAZEN, R.M. and WONES, D.R. (1978). Predicted and observed compositional limits of trioctahedral micas. Am. Mineral., 63, 885–892.

IMEOKPARIA, E.G. (1981): Distribution of ammonium in minerals of metamorphic and granitic rocks. Geochim. Cosmochim. Acta., 45, 983–988.

ISHII, M., SHIMANOUCHI, T. and NAKAHIRA, M. (1967): Far-infrared absorption spectra of layer silicates. Inorg. Chim. Acta, 1, 387–392.

ISHII, M., NAKAHIRA, M. and TAKEDA, H. (1969): Far-infrared absorption spectra of micas. Proc. Int. Clay Conf., 1, 247–259.

LAPERCHE, V. (1991): Étude de l'état et de la localisation des cations compensateurs dans les phyllosilicates. Thèse de 3ème cycle, Univ. Paris VII, 104 pp.

LEVILLAIN, C. (1982): Influence des substitutions cationiques et anioniques majeures sur les spectres Mössbauer et Infrarouge des micas potassiques trioctaédriques Applications cristallochimiques. Thèse d'Etat, Univ. Paris VI, 158 pp.

MANCEAU, A., BONNIN, D., STONE, W.E.E. and SANZ, J. (1990): Distribution of Fe in octahedral sheet of trioctahedral micas by polarised EXAFS. Comparaison with NMR results. Phys. Chem. Minerals., 17, 363–370.

MANNING, D.A.C. (1981): The effect of fluorine on liquidus phase relationships in the system Qz–Ab–Or with excess water at 1 kb. Contrib. Mineral. Petrol., 76, 206–215.

MASON, R. A. (1992): Models of order and iron-fluorine avoidance in biotite. Can. Mineral., 30, 343–354.

MUNOZ, J.L. (1984): F–OH and Cl–OH exchange in micas with applications to hydrothermal deposits. In: BAILEY, S.W. (ed.): Reviews in Mineralogy, 13, Micas, 469–493.

MUNOZ, J.L. (1969): Experimental control of fluorine reactions in hydrothermal systems. Am. Mineral., 54, 943–959.

MUNOZ, J.L. and LUDINGTON, S.D. (1974): Fluoride-hydroxyl exchange in biotite. Am. J. Sci., 274, 396–413.

PARRY, W.T., BALLANTYNE, G.H. and WILSON, J.C. (1978): Chemistry of biotite and apatite from a vesicular quartz latite porphyry plug at Bingham, Utah. Econ. Geol., 73, 1308–1314.

RAMBERG, H. (1952): Chemical bonds and the distribution of cations in silicates. J. Geol., 331–335.

RANCOURT, D.G (1994): Mössbauer spectroscopy of minerals II. Problem of resolving cis and trans octahedral Fe^{2+} sites. Phys. Chem. Minerals., 21, 250–257.

RANCOURT, D.G., KODAMA, H., ROBERT, J.-L., LALONDE, A.E. and MURAD, E. (1994): Accurate $^{[4]}Fe^{3+}$, $^{[6]}Fe^{3+}$ and $^{[6]}Fe^{2+}$ site populations in synthetic annite. Am. Mineral., 79, 51–62.

RANCOURT, D.G., PING, J.Y., BOUKILI, B. and ROBERT, J.-L. (1996): Octahedral-site Fe^{2+} quadrupole splitting distribution from Mössbauer spectroscopy along the (OH,F)-annite join. Phys. Chem. Minerals, 23, 63–71.

ROBERT, J.-L., BENY, J.-M. and VOLFINGER, M. (1989): Characterisation of lepidolites by Raman and Infrared spectrometries. Relation between OH-stretching wavenumbers and composition. Can. Mineral., 27, 225–235.

ROBERT, J.-L., BENY, J.-M., DELLA VENTURA, G. and HARDY, M. (1993): Fluorine in micas: crystal-chemical control of the OH-F distribution between trioctahedral and dioctahedral sites. Eur. J. Mineral., 5, 7–18.

RUTHERFORD, M.J. (1973): The phase relations of aluminous iron biotites in the system: $KAlSi_3O_8$–$KAlSiO_4$–Al_2O_3–Fe–O–H. J. Petrol., 14, 159–80.

SANZ, J. (1976): Ordre-désordre dans la couche octaédrique des micas trioctaédriques. Étude par résonance magnétique nucléaire, infrarouge et Mössbauer. Thèse, Univ. Cath. Louvain, Belgique.

SANZ, J. and STONE, W.E.E. (1979): NMR study of micas II. Distribution of Fe^{2+}, F^- and OH^- in the octahedral sheet of phlogopite. Am. Mineral., 64, 119–126.

SANZ, J. and STONE, W.E.E. (1983): NMR applied to minerals: VI. Local order in the octahedral sheet of micas: Fe-F avoidance. Clay Minerals, 18, 187–192.

TATEYAMA, H., SHIMODA, S. and SUDO, T. (1977): Estimation of K–O distance and tetrahedral rotation angle of K-micas from far-infrared absorption spectral data. Am. Mineral., 62, 534–539.

TISCHENDORF, G. (1973): Metallogenic basis of tin exploration in the Erzgebirge. Inst. Mining Metall., Sect. B82, B7–B24.

WEIDNER, J.R and MARTIN, R.F. (1987): Phase equilibria of a fluorine-rich leucogranite from the St. Austell pluton, Cornwall. Geochim Cosmochim. Acta, 51, 1591–1597.

WONES, D.R. (1963a): Phase equilibria of ferriannite $KFe^{2+}{}_3(Si_3Fe^{3+})O_{10}(OH)_2$. Am. J. Sci., 262, 918–929.

WONES, D.R. (1963b): Physical properties of synthetic biotites on the join phlogopite-annite. Am. Mineral., 48, 1300–1321.

WONES, D.R. and EUGSTER, H.P. (1965): Stability of biotite: experiment, theory and application. Am. Mineral., 50, 1228–1272.

ZAW, U.K. and CLARK, A.H. (1978): Fluoride-hydroxyl ratios of skarn silicates, Catung E-zone schellite orebody, Tungsten, Northwest Territories. Can. Mineral., 16, 207–221.

Manuscript received October 6, 1999: revision accepted October 11, 2000.